

## EXPERIMENTAL PROCEDURE

---

This chapter describes the experimental methods and techniques used in the present investigation in respect of synthesizing the composites and characterization of their physical, mechanical and tribological properties.

### 3.1 Raw materials

The following section highlights the procurement and chemical composition (as given by the supplier) of the different material used in the present study to synthesize the composites. The powders of Copper (purity- 99%; particle size -200 mesh) and Nickel (purity- 99%; particle size -200 mesh) were procured from Loba Chemie Pvt. Ltd., Mumbai, India whereas Titanium carbide powder (purity- 98%; particle size -325 mesh) supplied by Sigma Aldrich, Germany. The chemical compositions of Copper and Nickel powders, as provided by the suppliers are given in Tables 3.1 and 3.2, respectively.

**Table 3.1** Chemical composition of copper (Cu) powder

Element	Sb	As	Pb	Fe	Mn	Ag	Sn	Cu
wt.%	0.005	0.0002	0.05	0.005	0.005	0.005	0.005	balance

**Table 3.2** Chemical composition of nickel (Ni) powder

Element	Fe	S	C	Ni
wt.%	0.01	0.001	0.08	balance

Toluene or toluol is a colorless, water-insoluble liquid with the smell associated with paint thinners. Toluene ( $C_6H_5CH_3$ ) was used as a process control agent (PCA) to restrict the formation of any intermetallic compound during mixing was supplied by Ranbaxy, India.

### 3.2 Composite preparation

Conventional powder metallurgy technique has been used to synthesize the composites in the present study. Copper has been selected as the base metal whereas nickel was added to enhance the bonding between the matrix and TiC. Based on the literature, the amount of addition of Nickel was fixed at 4 wt. % and hence the Cu-4 wt. % Ni was used as the matrix alloy. Titanium carbide (TiC) was added in different amounts of 2, 4, 6 and 8% by weight. Hence, a total of five compositions namely, Cu-4wt.% Ni (Cu4Ni), Cu-4 wt.%Ni-2wt.%TiC (Cu4Ni-2TiC), Cu-4 wt.%Ni-4wt.% TiC (Cu4Ni-4TiC), Cu-4wt.%Ni-6wt.% TiC (Cu4Ni-6TiC) and Cu-4 wt.%Ni-8wt.% TiC (Cu4Ni-8TiC) were prepared in the investigation. The process flow chart for composite preparation is shown Fig.3.1.

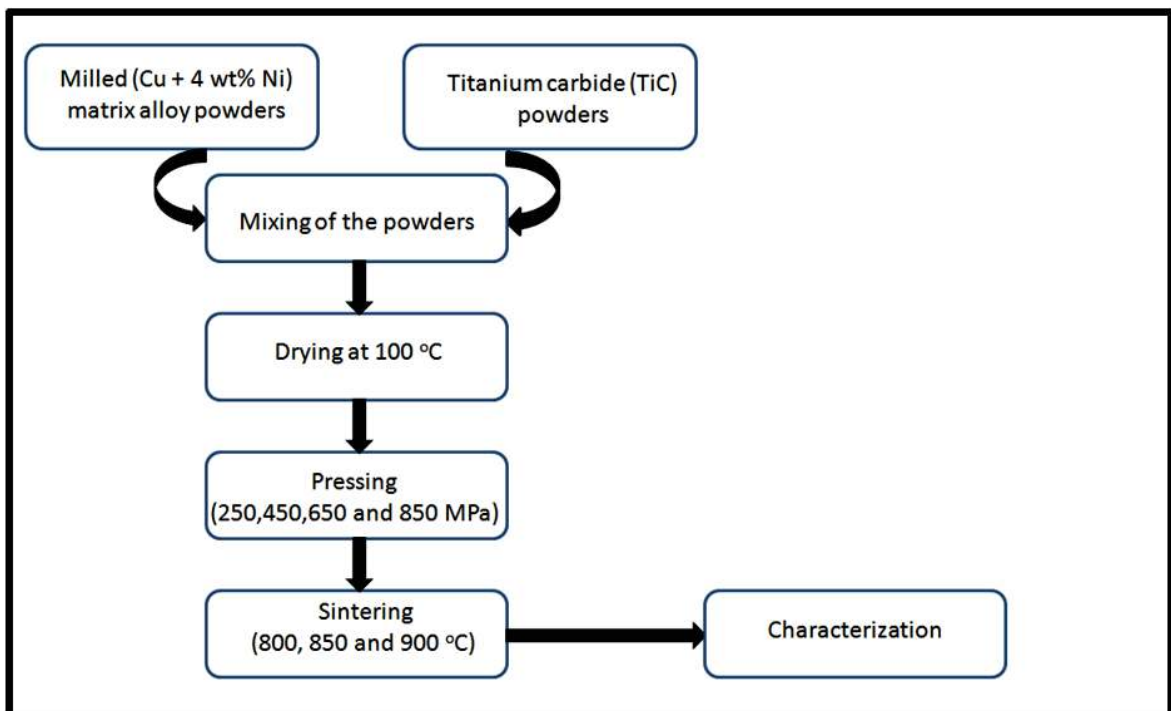


**Fig.3.1:** Process flow chart of the composite preparation and its characterization.

### **3.2.1 Blending**

The matrix alloy was produced by blending the copper powder and 4 wt.% nickel powder. This was done by using ball milling machine (Retsch, Verder Scientific Pvt. Ltd., Hyderabad, India). Zirconia balls were used as a grinding medium. The matrix alloy was reinforced with 2, 4, 6 and 8 wt.% TiC and the powder were ball milled for 8 h at 40 rpm. These blended powders were regarded as 0 h of the mechanically milled powders.

### **3.2.2 High-energy ball milling (Mechanical alloying) and drying**

The blended composite powders mentioned above were ground in a high-energy ball milling (V B Ceramics Consultants, Chennai, India) for 2, 4 and 6 h, respectively, in the presence of toluene which was added as a process control agent and to restrict the formation of intermetallic compounds during the milling process. Hardened stainless steel vial was used to seal the powders during milling and zirconia balls were used as grinding medium. The ball to powder ratio (BPR) was 10:1 and the speed was set at 400 rpm. The high- energy ball milling was stopped often for every 20 min and after that resumed for 20 min to avoid over- heating. The milled powders were dried for 1 h at 100°C to ensure that no moisture content left in the composite powders.

### **3.2.3 Pressing**

Powder pressing is the compaction of powders into a geometric form. Pressing is usually performed at room temperature. This creates a solid part called a green compact. In this investigation, the milled were compacted by cold uniaxial pressing in a rigid cylindrical die at a pressure of 250, 450, 650 and 850 MPa, respectively. The schematic diagram of the compaction press is shown in Fig. 3.2. The pressure was applied gradually during the preparation of pellets to avoid any crack formation in the pellets. Pressure at the end of the stroke was maintained for two minutes before its release. Stearic acid was used as a lubricant in the die, punch and butt for friction free movement. The compacted pellets were of 12 mm diameter and 2 mm thickness. These pellets were used to

determine the compressibility behavior of the powders. The final specimens of 12 mm diameter and 11 mm height were prepared at the optimized compaction pressure.

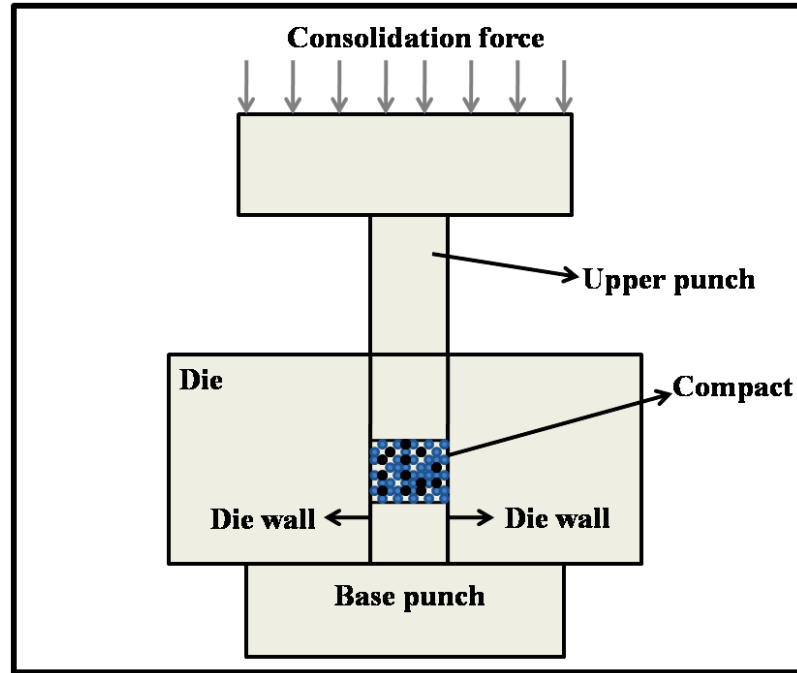


**Fig. 3.2:** Schematic diagram of the compaction press.

### 3.2.4 Sintering

After the compaction, the compacts were immediately taken out from the die set assembly and loaded into the furnace for sintering. Figure 3.3 shows the schematic diagram of the quartz tube furnace (Jupiter Engineering works, New Delhi, India) which was used for sintering purpose. It was a simple furnace having a quartz tube with maximum working temperature of 120°C. Glass wool was wrapped at the outside of the tube carefully so heat losses can be reduced. Gas inlet and outlets are provided to pass the argon gas through the furnace to prevent the oxidation of the samples during the sintering. A thermocouple (Type-K) was attached with the furnace to monitor the inner furnace temperature. The pellets were put in alumina crucibles which were then kept in furnace. The sintering was carried out in an inert gas (argon) atmosphere at three

different sintering temperature of 800°C, 850°C, 900°C, respectively, for a holding period of one hour with a heating rate of 5°C/min. The furnace was switched off after the completion of sintering with the specimens left inside the furnace and allowed to cool to room temperature. The specimens were then taken out of the furnace and cleaned by using a fine brush. Sintering temperatures were initially optimized in the range of 700-950 °C. It was observed that the specimens sintered at temperature below 800°C show poor densification and hardness because of incomplete sintering. However, we observed that the density as well hardness of specimens sintered at or beyond 850°C remained constant.

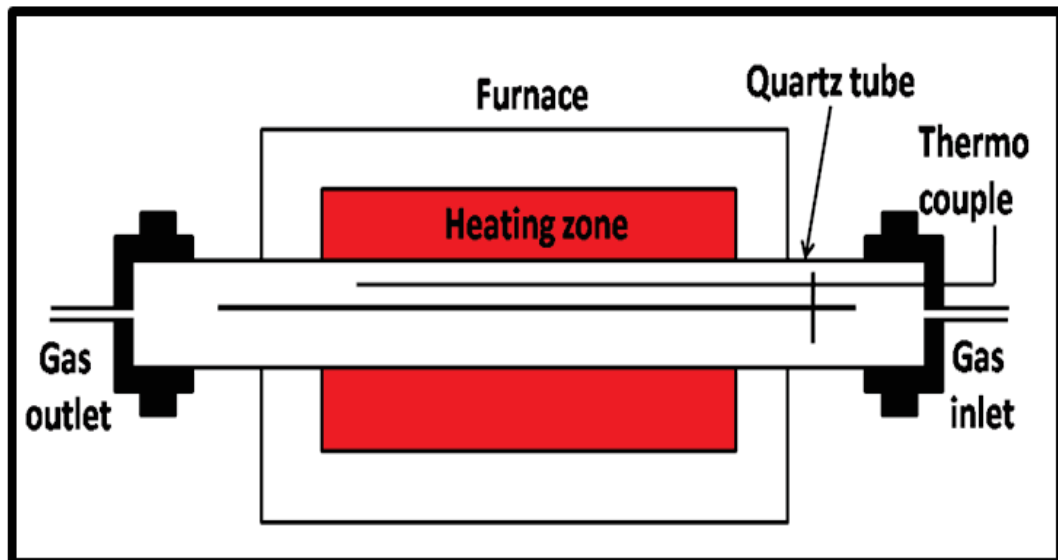


**Fig.3.3:** Schematic diagram of the furnace used in the present investigation.

### 3.3 Characterization of composites

The following sub-section describes the details of the procedures and techniques used to characterize the physical and mechanical behavior of the composites developed in the present study.

### 3.3.1 X-ray Diffraction analysis of composites

X-ray diffraction studies were carried out on both the powdered and sintered samples of the composites to determine the crystallite size, lattice strain, lattice parameter and phases present. X-ray diffraction (XRD) was performed by employing Rigaku Desktop Miniflex II X-ray diffractometer (Tokyo, Japan) using a Ni-filtered Cu-K $\alpha$  radiation ( $\lambda=1.5406\text{\AA}$ ) operated at 40 kV / 30 mA with a scanning speed of 2 $^\circ$ /min in the angle ( $2\theta$ ) range between 20–80 $^\circ$ . For all the intensity peaks and corresponding values of  $2\theta$ , the interplanar spacing,  $d$ , was calculated using Bragg's law given by Eq. 3.1, which is finally used for identification of various phases with the help of X-ray diffraction data cards (JCPDS)

$$2d \sin\theta = n\lambda \quad (3.1)$$

Where ' $\theta$ ' is the incident angle, ' $\lambda$ ' is the wavelength of the x-ray, and ' $n$ ' is an integer representing the order of the diffraction.

The crystallite size and lattice strain were determined using the standard Williamson–Hall equation given below (Williamson et al., 1953).

$$\beta_{hkl} \cos\theta_{hkl} = \left[ \frac{k\lambda}{t} \right] + 4\epsilon \sin\theta_{hkl} \quad (3.2)$$

Where  $k$  is the shape factor (0.9),  $\lambda$  is the wavelength of X-rays (1.5406  $\text{\AA}$ ),  $hkl$  are miller indices,  $\theta$  is the Bragg's angle,  $t$  is the crystallite size normal to the reflecting planes and  $\epsilon$  is the lattice strain. The first three Cu reflections (111), (200) and (220) were used to construct a linear plot of  $\beta_{hkl} \cos\theta_{hkl}$  against  $4\sin\theta_{hkl}$ . The crystallite size ( $t$ ) was obtained from the intercept,  $c$  (i.e.,  $c = k\lambda/t$ ), and the strain ( $\epsilon$ ) was determined from the slope (i.e.,  $m = \epsilon$ ). The results are presented in Chapter 4.

### 3.3.2 Electrical resistivity measurement

Electrical resistivity is an intrinsic property that quantifies how strongly a given material opposes the flow of electric current. A low resistivity indicates a material that readily allows the flow of electric current. Electrical resistivity of the composites having

different amounts of TiC was determined by a four-point probe tester (Keithley) at a room temperature. Pure indium metal was used for electrical contacts and platinum wires of 0.5 mm in diameter were used for connection. The measurements were taken using direct current. The contact points were prepared by adhesion with a thin layer of high conductivity silver paste. The samples had 9 mm in diameter and a length of 11 mm. In order to improve the contact, the junction points were polished by a fine grade emery sheet. The constant current ( $I = 0.5$  A), and the measurement of the voltage ( $V$ ), can be calculated using the relationship

$$V = IR \quad (3.3)$$

$$R = \rho \times L/A \quad (3.4)$$

where  $R$  is electrical resistance,  $\rho$  is electrical resistivity, and  $L$  and  $A$  are the length and cross-sectional area of specimens respectively.

### 3.3.3 Measurement of density of composites

Green density of different specimen was calculated by dividing weight of each pellet by its volume which was estimated from its dimension. The theoretical density of the compacts was calculated using rule of mixture. Sintered density of the compacts was also measured experimentally by using Archimedes method with the help of the calculated weight of compacts in air ( $W_a$ ) and in water ( $W_w$ ) using an electronic balance having an accuracy of 0.001g.

### 3.3.4 Hardness Measurement

Hardness is a measure of how resistant solid matter is to various kinds of permanent shape change when a compressive force is applied. The Vickers test is often easier to use than other hardness tests (Dieter, 2013). The hardness of all the specimens was measured by using an automated digital Vickers micro-hardness tester (Vaiseshika Electron Devices, Model: DHV-1000, India) at a constant load of 100 g and dwell time of

the 15s. At least ten indentations for hardness measurement were made at different locations and the average of these readings is reported.

### **3.4 Microstructural Studies**

For metallographic examination, samples were manually polished following the standard metallographic procedures described below. The surface of the specimen that is to be examined was first made plane by means of a specially designed motor-driven emery belt. The sharp edges of the specimen were then beveled to avoid the tearing of the emery paper in the subsequent polishing. The specimens were then polished manually using the SiC metallographic emery papers (120, 240, 400 and 600 grit). During polishing on each emery paper the direction of grinding was such as to introduce scratches at right angles to those introduced by the preceding paper. The final polishing is carried out on a sylvet-cloth using brasso and kerosene oil on a polishing machine (Bainpol, Metco, Chennai, India). After polishing, the specimens were etched using Ferric chloride ( $\text{FeCl}_3$ ), washed, dried and finally examined under optical microscope (Dewinter Opticals Inc., New Delhi, India). Typical microstructural features of all the samples are photographed.

The surface morphology of the samples was also examined under scanning electron microscope ZEISS (Model No. EVO/18), Germany, instrument operated at 5 kV and salient microstructural features were photographed. The specimens were also subjected to energy dispersive spectroscopy (EDS) to explore the compositional analysis. These optical and SEM micrographs and EDS patterns are presented and discussed in Chapter-4.

#### **High Resolution Scanning Electron Microscopy (HR-SEM)**

Morphological studies of sintered composite specimens were performed by high resolution-scanning electron microscope (HR-SEM) equipped with energy dispersive spectroscopy (Model No. NOVANANOSEM450). HR-SEM helps to better understand the bonding between the matrix alloy and reinforcement at a comparatively high resolution. The shape of the particles can also be observed through HR-SEM.



### 3.5 Dry Sliding Friction and Wear Testing

Dry sliding wear tests for the Cu-4wt.% Ni alloy and composites containing different amounts of TiC were carried out using a pin on disk apparatus (Magnum Engineers, Bangalore, India). Wear tests were conducted using cylindrical samples having 9 mm diameter and 11 mm height that had flat surfaces in the contact region and the rounded corner. The specimen was held stationary against the counterface of a 100 mm diameter rotating disc made of EN-31 steel hardened to 60 HRC as provided in the pin-on-disk machine at room temperature and 40-60% relative humidity. The composition of the material of the steel disc is given in Table 3.3. The EN-31 steel is a plain carbon steel case hardened to attain a hardness of 60 HRC.

**Table 3.3** Composition of EN-31 steel

Element	C	Si	Mn	S	P	Cr	Fe
wt.%	0.90-1.20	0.10-0.35	0.30-0.75	0.05	0.05	1.0-1.6	balance

The load was applied to the specimen through the lever resulting in a continuous contact between the pin and the counter face. The schematic diagram of the pin on disk apparatus is shown in Fig.3.4. The contact surface of specimens was polished with emery papers of 1/0, 2/0, 3/0 and 4/0 grade and cleaned with acetone prior to conducting the wear tests. The tests were conducted under four different normal loads of 5, 10, 15 and 20 N and three sliding speeds of 0.75, 1 and 1.25 m/s. Wear tests were conducted for a total duration of 30 min and the weight loss was measured at the intervals of 5 min. To measure the weight loss, the specimen was removed from the holder after 5 min of run, cooled to room temperature, brushed lightly to remove loose wear debris, weighed and fixed again in exactly the same position in the holder so that the orientation of the sliding surface remained unchanged. The weight was taken using an analytical balance having an accuracy of  $1 \times 10^{-7}$  kg. Weight loss data was converted to volume loss data using the density of respective composite as measured by Archimedes' principle density. Each test at a given load and sliding velocity has been repeated three times and the average data for volume loss after each interval of time has been reported. The machine had a control panel

showing the frictional force, hence, the friction force was noted every 30 sec and the same was used to calculate the coefficient of friction by dividing it by normal load.

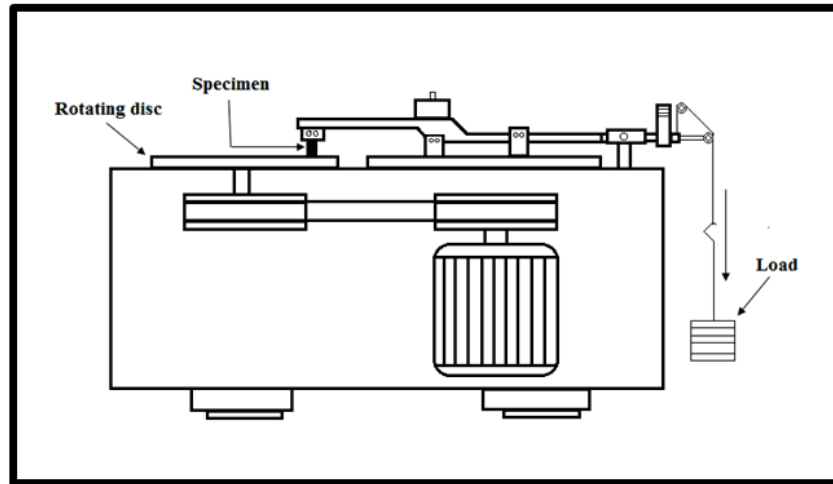


**Fig.3.4:** Schematic diagram of the pin on disk testing rig.

Mathematically, coefficient of friction can be obtained by using the formula

$$\mu = \frac{F}{N} \quad (3.5)$$

Where  $\mu$  is the coefficient of friction,  $F$  is the frictional force and  $N$  is the normal load. This helped in plotting the variation of friction coefficient with sliding distance. The data for friction coefficient was then averaged over sliding distance to get an average coefficient for a particular test and this has been used in analyzing the variation of friction with either load or composition.

### 3.6 Examination of worn surfaces

In order to explore the prevailing mechanisms of wear, the sliding surfaces of Cu-4wt.%Ni alloy and Cu-4wt.% Ni based composites containing different amounts of TiC, worn under each test condition were examined under scanning electron microscope (SEM) ZEISS, EVO/18, Germany, and the salient features in each were photographed.